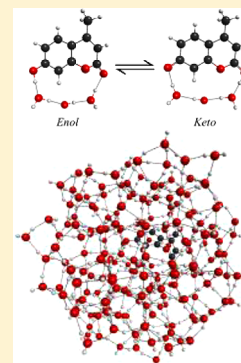# Excited-State Hydrogen Atom Transfer Reaction in Solvated 7-Hydroxy-4-methylcoumarin

Nuwan De Silva, Noriyuki Minezawa, and Mark S. Gordon*

Department of Chemistry, Iowa State University, Ames, Iowa 50011, United States

ABSTRACT: Excited-state enol to keto tautomerization of 7-hydroxy-4-methylcoumarin (C456) with three water molecules (C456:3H$_2$O), is theoretically investigated using time-dependent density functional theory (TDDFT) combined with the polarizable continuum model and 200 waters explicitly modeled with the effective fragment potential. The tautomerization of C456 in the presence of three water molecules is accompanied by an asynchronous quadruple hydrogen atom transfer reaction from the enol to the keto tautomer in the excited state. TDDFT with the PBE0 functional and the DH(d,p) basis set is used to calculate the excited-state reaction barrier height, absorption (excitation), and fluorescence (de-excitation) energies. These results are compared with the available experimental and theoretical data. In contrast to previous work, it is predicted here that the coumarin 456 system undergoes a hydrogen atom transfer, not a proton transfer. The calculated reaction barrier of the first excited state of C456:3H$_2$O with 200 water molecules is found to be −0.23 kcal/mol without zero-point energy (−5.07 kcal/mol with zero point energy, i.e., the activation energy).

1. INTRODUCTION

The hydrogen atom transfer/proton transfer (HT/PT) reaction is one of the most fundamental reactions occurring in chemistry and biology.[1−6] For example, the excited-state HT/PT relay along the hydrogen-bonded network is a vital reaction in revealing the photoreactivity in green fluorescent protein,[7,8] which is widely used for fluorescence markers in living cells to illuminate a function of a specific gene. The multiple proton relay also plays a critical role in a proton pump across a cell membrane through the proton wire, where the proton transport is achieved against a pH gradient in and out of the membrane. The mechanism of proton transport is also a significant aspect in developing novel polymer electrolyte fuel cells and direct methanol fuel cells, where the multiple proton relay in the water networks may proceed via the Grotthuss mechanism.[9] A full understanding of the mechanisms and dynamics of HT/PT reactions is, therefore, of great importance.

HT/PT reactions can occur either as an intramolecular reaction in which the donor and acceptor groups exist within the same molecule or as an intermolecular reaction in which the donor and acceptor groups are in two different molecules. However, the intramolecular HT/PT reaction cannot spontaneously occur in some molecules because the proton acceptor is not close enough to the proton donor. In such a case, solvent molecules may assist the HT/PT reaction (pseudo-intermolecular reaction) via hydrogen bond formation between the donor and the acceptor and conducting the donor hydrogen atom or proton to the acceptor. Therefore, in the presence of solvent assistance, the formation of hydrogen bonds along the reaction coordinate can induce a relay of multiple protons or hydrogen atoms from the reactants to the products. However, it is difficult to experimentally determine the characteristic features in a multiple-HT/PT mainly because of thermal fluctuations in the reaction center in the condensed phase.

Often, HT/PT reactions are encountered in the excited state. Research on excited-state HT and PT (ESHT and ESPT) reactions at the molecular level can be complex due to the structural complexity, very short time scales, and solvent fluctuations involved in the process. Upon electronic excitation, the geometry and acid–base characteristics of a molecule are significantly modulated if ESHT/ESPT occurs. Because the HT/PT process involves motion of the hydrogen atom or proton, the HT/PT transfer process is very sensitive to the degree of hydrogen bonding and also to the dielectric properties of the solvent. Therefore, HT/PT reactions in aqueous solution may involve different reaction pathways and dynamics, depending on the reactants, number of water molecules, and their relative orientations.

Excited-state double HT/PT was discovered by Kasha and co-workers[10] for 7-azaindole (7AI) in alcohol complexes and in a doubly hydrogen-bonded 7AI dimer formed in high concentrations in nonpolar solvents. Since then, the photophysics of bifunctional heteroaromatic compounds has received a great deal of attention. Supersonically jet-cooled hydrogen-bonded clusters in the gas phase are good model systems to reveal the dynamics of multiple-HT/PT, where the lowering of the temperature significantly suppresses the thermal fluctuations and the cluster size can be controlled.[11] Theoretically, simple model compounds of certain molecules with appropriate protic solvents have been studied to understand the HT/PT process. Kyrychenko et al.[12] have studied the HT/PT reaction of 1H-pyrrolo[3,2-h]quinolone (PQ) with one and two water molecules in the lowest excited singlet states at the TDB3LYP/cc-pVDZ level in the gas phase. They have calculated the ESPT

reaction barrier to be 20.9, 3.0, and 5.6 kcal/mol, respectively, for PQ, PQ:1H$_2$O, and PQ:2H$_2$O. Leutwyler and co-workers[13] performed CIS/6-31G(d,p) calculations to investigate the possible competition between HT and PT in 7-hydroxyquinoline (7HQ) with three NH$_3$ molecules. They found that the barrier for the PT reaction path is 20−25 kcal/mol higher than that for the HT path. Fernandez-Ramos et al.[14] performed complete active space self-consistent field (CASSCF) and multiconfiguration second-order perturbation theory (CASPT2) calculations with the 6-31G(d,p) basis set to investigate the enol to keto tautomerization in the lowest singlet excited state of 7HQ with three NH$_3$ molecules with C_s symmetry in the gas phase. The CASPT2//CASSCF energy barrier for the HT process is ∼5 kcal/mol, while the predicted PT pathway has a much larger energy barrier of ∼20 kcal/mol.

An early theoretical study on the ESHT reaction of 7AI:1H$_2$O was performed by Chaban and Gordon,[15,16] in which the CASSCF/DZP method was used for the isolated 7AI molecule and the 7AI:1H$_2$O complex in the ground and first excited states. 7AI was predicted to be more stable than the tautomer in the ground state, whereas the relative energies are reversed in the excited state, and the activation energies for tautomerization in both states of 7AI are significantly reduced by the complexation with water.

Most coumarin (1,2-benzopyrone) derivatives have relatively high fluorescence quantum yields.[17−22] Consequently, they are widely used as fluorescent indicators, laser dye colorants, nonlinear optical chromophores, and excellent probes to study the solvation dynamics.[23−29] Among the coumarin dyes, hydroxycoumarin dyes have received the most attention because of their interesting anomalous pH-dependent fluorescence spectra.[30−34] For example depending on the acidity of the solvent, 7-hydroxy-4-methylcoumarin (4-methylumbelliferone), also commercially known as coumarin 456 (C456), exhibits a variety of fluorescence spectra that have been suggested as the basis for the construction of acidity-tunable blue−green lasers.[31,32,34] Henceforth, coumarin 456 will be referred to as C456. C456 is a fluorescent indicator that is colorless at pH 7.0 and exhibits a blue fluorescence at pH 7.5.

Electronic excitation to the S$_1$ state strongly modifies the acid−base properties of C456, rendering the hydroxyl group more acidic (S$_0$ (pK_a = 7.26), S$_1$ (pK_a ≈ 0.45)).[35] C456 is a fluorescence indicator and a laser dye whose emission range is exceptionally broad (360−590 nm). In the excited state, C456 exhibits four possible fluorescent species, depending on the solvent and the pH, enol (E*, 380 nm), anionic (A*, 450 nm), cationic (C*, 412 nm), and keto-tautomeric (K*, 480 nm). In the ground state, on the other hand, the absorption spectra indicate only three species, enol (E), anion (A), and cation (C).[36−38] Therefore, the K* form appears to be an excited-state reaction product, which arises from the E* form through HT/PT from the donor (acidic O−H) to the acceptor (basic C=O) group in the excited state. Direct intramolecular HT/PT in C456 would be difficult because the donor and acceptor components are too far away from each other. Therefore, C456 requires a solvent wire to bridge the donor and acceptor groups. Two different mechanisms of photoexcited tautomerization processes have been discussed in the literature,[33,36,37,39] a dissociative two-step pathway[33,39] via the A* or C* species (reaction intermediates) and a nondissociative[36,37] one-step reaction in water. The latter is considered to be the most probable mechanism.

C456 has been investigated theoretically[40] using the TDB3LYP method and the resolution-of-the-identity coupled cluster singles and doubles (RI-CC2) method with the SVP, SVPD, TZVP, and TZVPD basis sets. The excitation and de-excitation energies of the lowest singlet states for the enol and keto forms were studied in the gas phase and in solution using the polarizable continuum model (PCM)[41,42] for water. The calculations revealed that in the PCM of water, the π−π* state is the lowest-lying excited state. Georgieva et al. extended the investigation by studying the PT reaction in C456 along a H-bonded water wire of three water molecules using TDDFT, RI-CC2, and singly excited configuration interaction (CIS) calculations.[43] The calculations suggest the possibility of HT/PT from the enol to the keto form in the excited state. All of the methods used predict that the reaction path occurs in the π−π* state, and no crossing with a Rydberg-type πσ* state was found. The calculations predict that the S$_1$ enol and keto clusters are separated by a barrier height of 17−20 kcal/mol, although an actual transition-state structure was not determined.

In this paper, the excited-state quadruple HT/PT reaction of C456 with three quantum water molecules (C456:3H$_2$O) has been studied. Solvent effects are analyzed by incorporating both the PCM model and the effective fragment potential (EFP) for water.[44−46]

2. COMPUTATIONAL DETAILS

The geometries of the enol and keto tautomers of C456 in the ground state (E and K) and the π−π* first excited state (E* and K*) were optimized using PBE0 and TDPBE0,[47−49] respectively, with the DH(d,p)[46] basis set, with no symmetry constrains (C_1 symmetry). The enol tautomer, transition state (TS), and keto tautomer of C456:3H$_2$O as well as C456:3H$_2$O with small clusters of EFP water molecules (C456:3H$_2$O + nEFP, n = 1−4) in the ground state (E, TS, and K) and the π−π* first excited state (E*, TS*, and K*) were also optimized using the same levels of theory. The geometry optimizations converged the gradient to less than 0.0001 hartree/bohr. The Hessian (matrix of energy second derivatives) was calculated and diagonalized at the optimized geometries. All E, K, E*, and K* stationary points of C456, C456:3H$_2$O, and C456:3H$_2$O + nEFP were characterized as true minima by confirming that all corresponding eigenvalues of the Hessian are positive. The TS and TS* stationary points were characterized as true saddle points by confirming that there is just one negative Hessian eigenvalue.

The reaction paths in the ground state (S$_0$) and the first π−π* excited state (S$_1$) for C456:3H$_2$O and C456:3H$_2$O + nEFP were determined by calculating the intrinsic reaction coordinates (IRC),[50−55] starting from the corresponding TSs. The IRC is the steepest-descent path in mass-weighted coordinates and is calculated by propagating the system from the TS backward and forward toward the reactants (enol tautomer) and products (keto tautomer), respectively.

An additional interpretive tool is provided by the electrostatic potential (ESP)-derived[56,57] TDPBE0/DH(d,p) atomic charges along the excited-state IRC path (30 equally spaced points) to determine whether the S$_1$ reaction is primarily HT or PT in the C456:3H$_2$O system.

The C456 and C456:3H$_2$O systems in the presence of PCM water are denoted C456:PCM and C456:3H$_2$O + PCM, respectively, throughout the remainder of the paper. The stationary points of C456:PCM (E, E*, K, and K*) and C456:3H$_2$O + PCM (E, E*, TS, TS*, K, and K*) were fully optimized and characterized in both S$_0$ and S$_1$. The S$_0$ and S$_1$ IRC paths of C456:3H$_2$O + PCM were also generated.

The Monte Carlo (MC)[58,59] with simulated annealing (SA)[60] method was used to sample the potential energy surface of C456:3H$_2$O with 200 EFP water molecules (C456:3H$_2$O + 200EFP) in S$_0$ and S$_1$ using PBE0/DH(d,p) and TD-PBE0/DH(d,p),
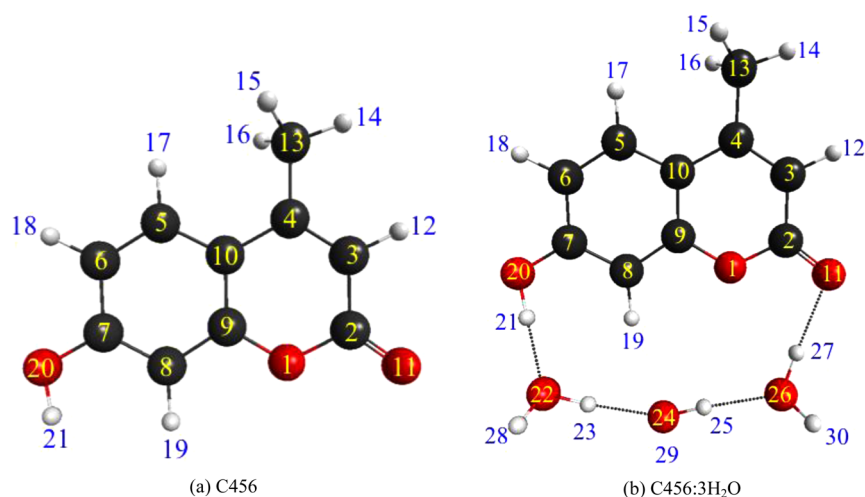
Figure 1. The atom labeling of (a) C456 and (b) C456:3H$_2$O.

respectively. The gas-phase optimized geometries of C456:3H$_2$O and C456:3H$_2$O + nEFP were used as the starting geometries of the MC/SA simulations with 200 EFP water molecules. The MC/SA method with local minimization was used to sample the configuration space. For each global minimum found, the number of structures sampled was on the order of 100000−350000. The number of steps taken for each temperature varied from 10 to 1000. The number of steps between local optimizations varied from 10 to 100. The number of fragments moved per step varied from 1 to 20. The starting temperature for the SA varied from 20000 to 1000 K, and the final temperature varied from 100 to 300 K.
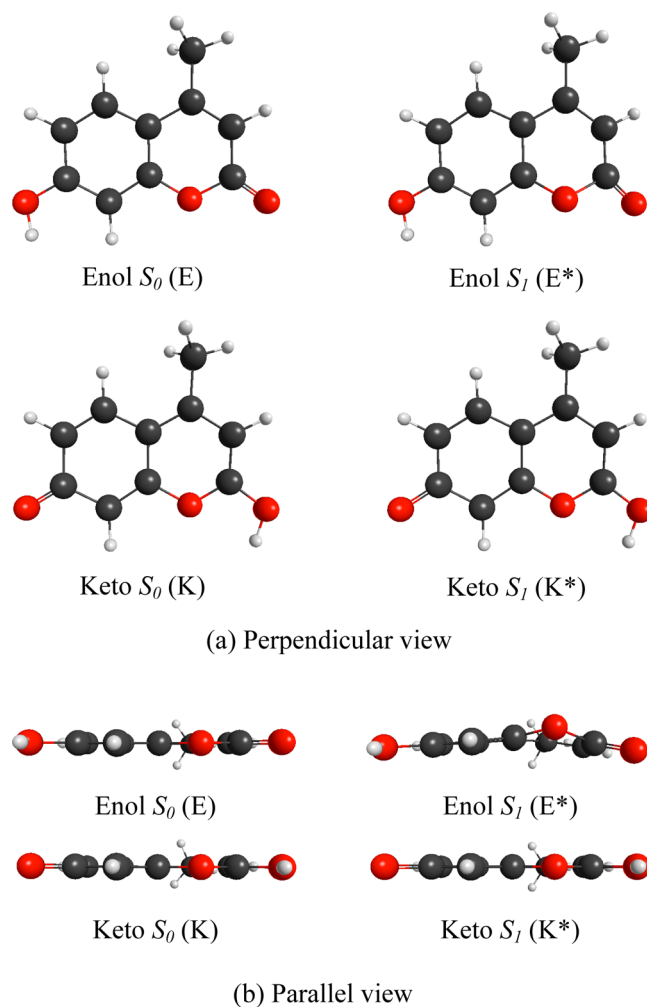
To obtain the tautomerization activation energy, zero-point energy (ZPE) corrections have been obtained using the harmonic frequencies. The S$_0$ tautomerization barrier height, without ZPE corrections, is $E_{b(E \to K)} = E_{TS}(S_0) - E_E(S_0)$, where the subscript E refers to the enol tautomer. The barrier height with ZPE corrections yields the 0 K activation energy, $E_{a(E \to K)}$. The barrier height and activation energy in the S$_1$ excited state are obtained in an analogous manner. These two quantities are denoted as $E_{b(E^* \to K^*)}$ and $E_{a(E^* \to K^*)}$, respectively.

Using the optimized geometries, vertical and adiabatic excitation energies (absorption) and vertical de-excitation energies (fluorescence) were carried out with TDPBE0/DH(d,p). Only singlet-to-singlet transitions are considered here. The vertical excitation energy corresponds to the electronic excitation from the ground-state minimum (S$_0$) to the first electronic excited S$_1$ state ($\pi\pi^*$), with no geometry relaxation. The adiabatic excitation energy is the energy difference between the minimum on the S$_1$ surface and the minimum on the S$_0$ surface. The vertical de-excitation energy corresponds to the energy difference between the S$_0$ and S$_1$ states at the S$_1$ minimum-energy geometry. The ZPE corrections to the adiabatic excitation energies were obtained using the ZPEs of the corresponding minima.

All calculations were performed with the general atomic and molecular electronic structure system (GAMESS).[61,62] The structures were visualized with MacMolPlot,[63] a graphical interface to GAMESS.

3. RESULTS AND DISCUSSION

The atom labeling of the C456 and C456:3H$_2$O are illustrated in Figure 1. The C456-optimized geometries of the stationary points of S$_0$ (E and K) and S$_1$ (E* and K*), optimized with PBE0/DH(d,p) and TDPBE0/DH(d,p), respectively, are shown in Figure 2. Except


Enol S_0 (E) Enol S_1 (E*)

Keto S_0 (K) Keto S_1 (K*)

(a) Perpendicular view

Enol S_0 (E) Enol S_1 (E*)

Keto S_0 (K) Keto S_1 (K*)

(b) Parallel view

Figure 2. The optimized geometries of the C456 stationary points of S$_0$ (E, TS, and K) and S$_1$ (E*, TS*, and K*) optimized, respectively, with PBE0/DH(d,p) and TDPBE0/DH(d,p). The molecular geometry is shown in two different views (directions) relative to the molecular fused-ring plane: (a) perpendicular view and (b) parallel view.

for the position of the enol (O20−H21) and keto (C2−H11) functional groups, the main structural difference between the two tautomers is the ring nonplanarity of the S$_1$ state; the E* tautomer is nonplanar (O1 oxygen atom located out of the fused ring plane)
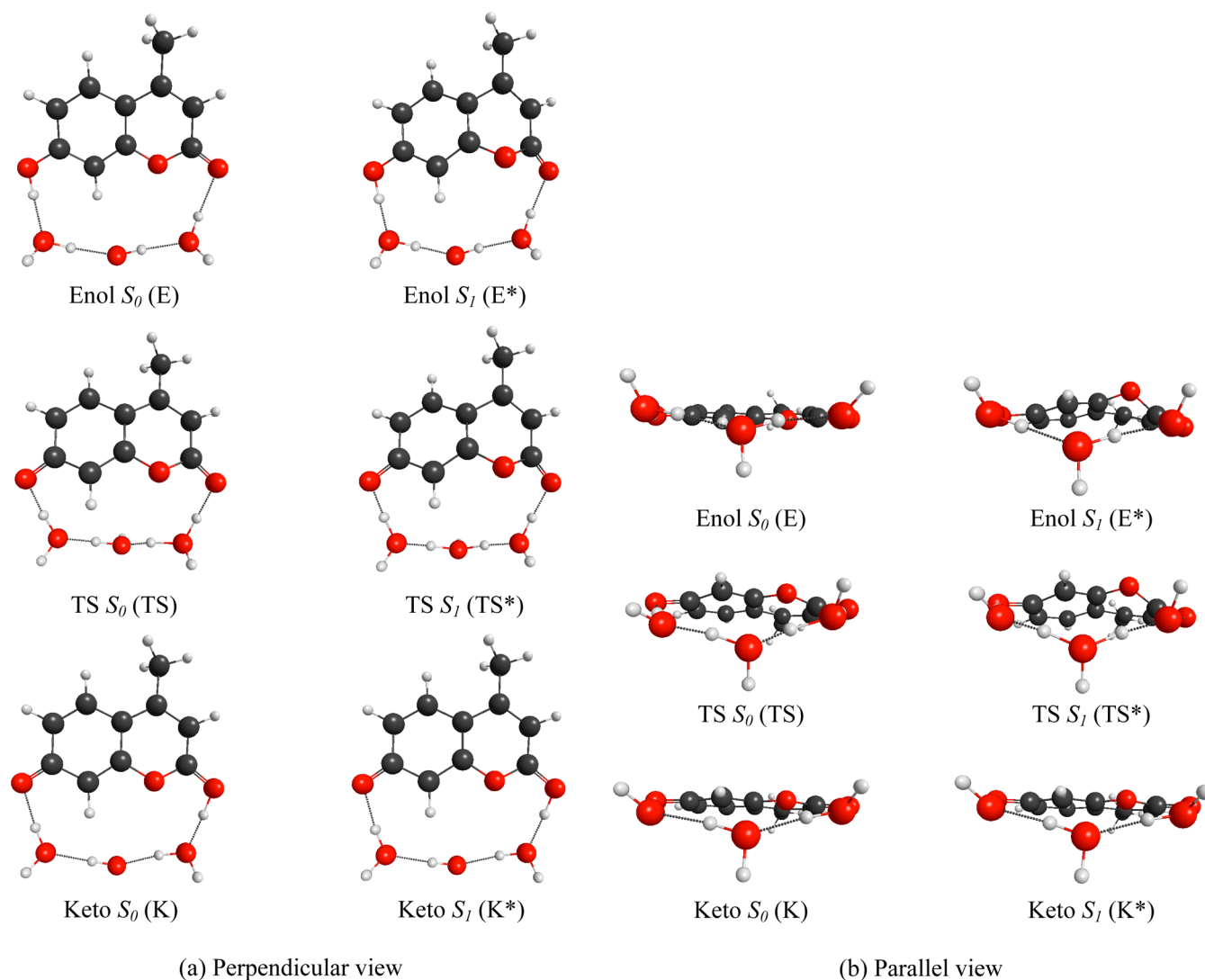
Figure 3. The geometries of the stationary points of S_0 (E, TS, and K) and S_1 (E*, TS*, and K*) of C456:3H$_2$O optimized, respectively, with PBE0/DH(d,p) and TDPBE0/DH(d,p). The molecular geometry is shown in two different views (directions) relative to the molecular fused-ring plane: (a) perpendicular view and (b) parallel view.
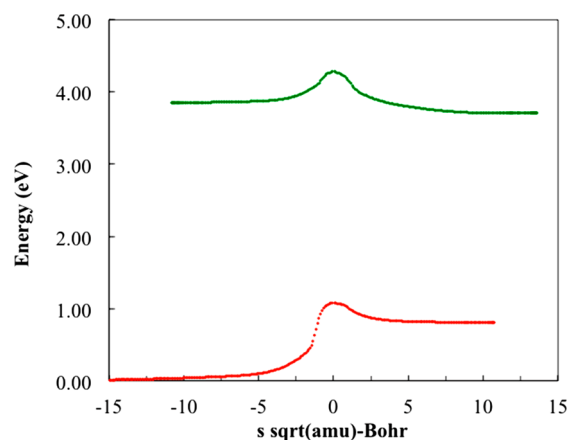
Figure 4. The IRC path in the ground state (red) and the first $\pi-\pi*$ excited state (green) of C456:3H$_2$O calculated with PBE0/DH(d,p) and TDPBE0/DH(d,p), respectively, starting from the corresponding TSs.

Table 1. 0 K Relative Enthalpies (H_{rel}^0) of the C456 Tautomers^a

	S_0		S_1	
	enol	keto	keto	enol
C456	0.00 (0.00)	1.09 (1.11)	3.67 (3.77)	3.90 (4.05)
C456:3H$_2$O	0.00 (0.00)	0.77 (0.80)	3.58 (3.71)	3.72 (3.85)
C456:PCM	0.00 (0.00)	0.93 (0.95)	3.68 (3.78)	3.71 (3.81)
C456:3H$_2$O + PCM	0.00 (0.00)	0.70 (0.71)	3.54 (3.64)	3.59 (3.68)
C456:3H$_2$O + 200EFP	0.00 (0.00)	0.24 (0.27)	3.22 (3.34)	3.47 (3.60)

^{a}The relative energies are given relative to the S_0 state of the enol tautomer. The values in parentheses are relative energies without ZPE correction (E_{rel}). All values are given in eV.

relative to the E, K, and K* tautomers. The ZPE-corrected relative 0 K enthalpies (H_{rel}^0) and relative energies without the ZPE correction

(E_{rel}) of the C456 tautomers are given in Table 1. According to Table 1, H_{rel}^0 of the enol tautomer of C456 is lower in energy than that of keto in S_0 by 1.09 eV (25.14 kcal/mol). In contrast H_{rel}^0 of the keto tautomer of C456 is lower in energy in the excited state by 0.23 eV (5.30 kcal/mol). Therefore, the enol to keto tautomerization of C456 is highly endothermic in S_0 and exothermic in S_1. The favorable thermodynamics in S_1 is one of the reasons that the enol to keto tautomerization reaction occurs most likely in the S_1 state.

The relative energy of enol in S_0 and keto in S_1 holds for the other C456 complexes in Table 1. The keto–enol energy difference in S_1 is

Table 2. S_0 and S_1 0 K Activation Energies ($E_{a(E\rightarrow K)}$ and $E_{a(E^*\rightarrow K^*)}$) of the Enol → Keto Tautomerization of the C456 Complexes[a]
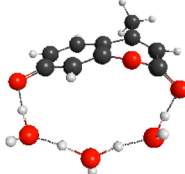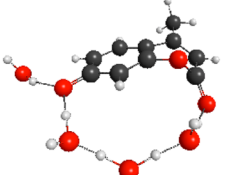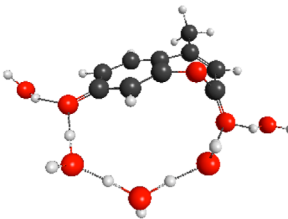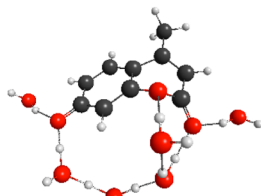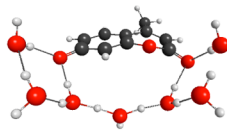
	S_0	S_1
C456:3H$_2$O	0.87 (1.09)	0.23 (0.44)
C456:3H$_2$O + PCM	0.70 (0.84)	0.20 (0.29)
C456:3H$_2$O + 200EFP	0.44 (0.66)	−0.22 (−0.01)

[a]The energies without ZPE corrections are given in parentheses. All values are given in eV.

generally rather small, ranging from 0.23 eV when no water is present to 0.03 and 0.05 eV for C456:PCM and C456:3H$_2$O + PCM, respectively. The most important factor for a probable S_1 tautomerization is the lower activation energy compared to the S_0 activation energy (Table 2). The location of a TS was unsuccessful for the isolated C456 system due to the long distance between H21 and O11 (~7 Å) in the enol structure and the similarly in the keto structure (see Figure 1).

In order to locate the C456 TS, three quantum water molecules were spatially arranged to bridge the two functional groups via hydrogen bonding. Then, fully optimized TSs were obtained in both the S_0 and S_1 states. C456 requires a minimum

Table 3. Excited-State Activation Energy (eV), $E_{a(E^*\rightarrow K^*)}$, of the Enol → Keto Tautomerization Reaction of C456:3H$_2$O + nEFP[a]

n	i	$E_{a(E^*\rightarrow K^*)}$	TS*
0	629	0.23 (0.44) [0.38]	
1	541	0.12 (0.33) [0.33]	
2	492	0.11 (0.32) [0.33]	
3	599	−0.02 (0.19) [0.21]	
4	353	−0.17 (0.04) [0.07]	

[a]The barrier height, $E_{b(E^*\rightarrow K^*)}$ is given in parentheses. The barrier heights, $E_{b(E^*\rightarrow K^*)}$ calculated using the single-point energies on the above structures with PCM are given in square brackets. The imaginary frequency (i) of the TS* is given in cm^{-1}.

of three water molecules (C456:3H$_2$O) to find the enol to keto tautomerization TS. The TS searches for C456 with one, two, and four water molecules were not successful. One and two waters are not sufficient to bridge the two functional groups within C456, while four waters makes the bridge too crowded. The C456:3H$_2$O optimized geometries of the S$_0$ (E, TS, and K) and S$_1$ (E*, TS*, and K*) stationary points, optimized, respectively, with PBE0/DH(d,p) and TDPBE0/DH(d,p), are given in Figure 3. In general, the S$_1$ state C456:3H$_2$O stationary points are somewhat more nonplanar than those of the S$_0$ state. The TS and TS* imaginary frequencies are 629i and 601i cm^{-1}, respectively. The IRC paths for the S$_0$ and S$_1$ states are shown in Figure 4. Each IRC path confirms that the corresponding TSs do connect the reactants and products as expected. When going from the reactant to the products, four bonds (including three hydrogen bonds) are broken, and four bonds are formed, asynchronously along the reaction coordinates.

The ESP-derived charges are shown in Figure 5 according to the atom labeling in Figure 1. The ESP-derived charges in the excited state enable one to assess whether PT or HT occurs during the E* to K* tautomerization. According to Figure 5,
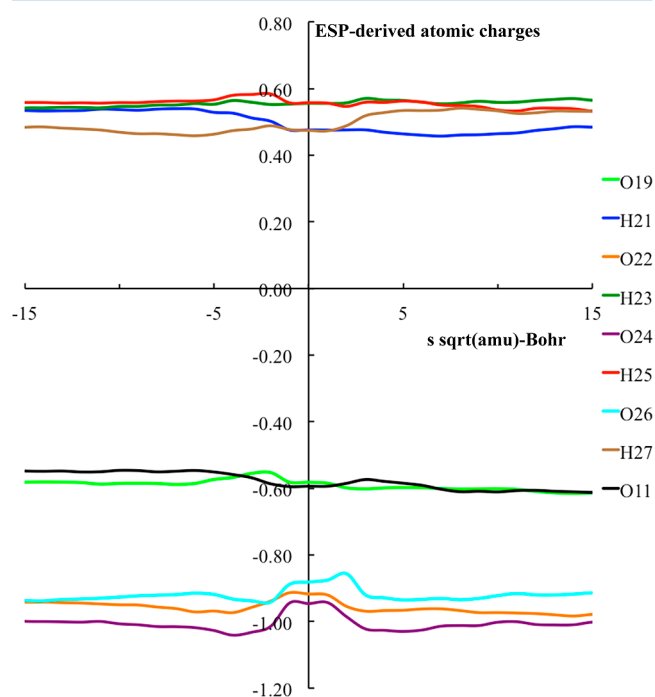
Figure 5. The ESP-derived TDPBE0/DH(d,p) atomic charges on the O20, H21, O22, H23, O24, H25, O26, H27, and O11 atoms along the IRC path of the S$_1$ state of C456:3H$_2$O.

the ESP-derived atomic charges on the atoms O20, H21, O22, H23, O24, H25, O26, H27, and O11 do not change significantly on the C456:3H$_2$O S$_1$ IRC path. However, the charges on atoms O22, O24, and O26 increase from $\sim$−1.0e to $\sim$−0.9e just before the TS and then decrease again just after the TS. Moreover, the overall charge on H21 decreases, and the overall charge on H27 increases by $\sim$0.1e before (enol) and after the reaction (keto). It is interesting to note the charge of the intermediate H23 and H25 transferring atoms in the TS. The charges on these atoms hardly change throughout the reaction path, remaining at $\sim$0.55e. This is close to the partial charge on a H atom in a water molecule, as compared to a proton charge of +1. Therefore, the enol−keto excited-state

process corresponds to a HT, not a PT. This is in good agreement with the CIS/SVPD population analysis done by Georgieva et al.[43] on C456:3H$_2$O, where for the S$_1$ ($\pi\pi*$) state charges of 0.61e for H23 and H25 have been found. The CIS/6-31(+)G(d,p) population analysis done by Tanner et al.[11,13,64] on 7HQ(NH$_3$)$_3$ predicted for the S$_1$ ($\pi\pi*$) state a charge of 0.70e for the NH$_4$ moiety. Therefore, the S$_1$ state enol to keto tautomerization reaction of C456:3H$_2$O can be interpreted as an asynchronized quadruple HT reaction, even though the transferring H atoms carry substantial partial charges.

The activation energies for the HT from the E to the K tautomeric form in C456:3H$_2$O, C456:3H$_2$O + PCM, and C456:3H$_2$O + 200EFP complexes are given in Table 2. Table 2 indicates that the S$_0$ tautomerization of C456:3H$_2$O in the gas phase is characterized by a high activation energy (0.87 eV), whereas the S$_1$ state reaction proceeds with a low activation energy (0.23 eV). The inclusion of a small cluster of water molecules decreases the tautomerization activation energy in the S$_1$ state (Table 3). Moreover, HT in the excited state C456:3H$_2$O + 200EFP is predicted to proceed through a significantly lower activation energy (−0.22 eV with ZPE correction) in the S$_1$ state. A negative activation energy indicates a barrierless process. The S$_0$ state activation energy in C456:3H$_2$O + 200EFP also decreases two-fold compared to that of the C456:3H$_2$O. The effect of adding PCM on the C456:3H$_2$O S$_0$ and S$_1$ activation energies is small.

The excited-state HT activation energies of C456:3H$_2$O + nEFP (n = 1−4) are given in Table 3. In the C456:3H$_2$O + nEFP complexes, the energy barrier is dramatically reduced compared to C456:3H$_2$O, so that upon excitation of the C456:3H$_2$O + nEFP complex, the tautomerization can occur rapidly. Therefore, the hydrogen bond interaction between the EFP molecules and the bridging quantum water molecules

Table 4. TDPBE0/DH(d,p) Vertical Excitation (Absorption), Adiabatic, and Vertical De-excitation (Fluorescence) Energies for the C456 Enol Tautomer[a]

enol tautomer	vertical	adiabatic	fluorescence	exp
C456	4.28	3.90 (4.05)	3.58	3.88[b]
C456:3H$_2$O	4.04	3.72 (3.85)	3.05	
C456:PCM	4.17	3.71 (3.81)	3.62	
C456:3H$_2$O + PCM	4.03	3.59 (3.68)	3.31	
C456:3H$_2$O + 200EFP	4.15	3.47 (3.60)	3.00	

[a]All energies are given in eV. The adiabatic energies are given with the ZPE correction. The values in parentheses are the adiabatic energies without the ZPE correction. [b]Absorption energy of the enol tautomer of C456 in benzene.[36]

Table 5. TDPBE0/DH(d,p) Vertical Excitation (Absorption), Adiabatic, and Vertical De-excitation (Fluorescence) Energies for Keto Tautomer of C456[a]

keto tautomer	vertical	adiabatic	fluorescence	exp
C456	3.02	2.59 (2.66)	2.27	3.33[b]
C456:3H$_2$O	3.20	2.81 (2.90)	2.52	
C456:PCM	3.18	2.75 (2.83)	2.59	
C456:3H$_2$O + PCM	3.24	2.84 (2.93)	2.71	
C456:3H$_2$O + 200EFP	3.64	2.98 (3.07)	3.04	

[a]All energies are given in eV. The adiabatic energies are given with the ZPE correction. The values in parentheses are the adiabatic energies without the ZPE correction. [b]Fluorescence energy of the keto tautomer of C456 in benzene.[36]

further decreases the activation energy. For the C456:3H$_2$O + 4EFP system, following the IRC along the reaction that is referenced in Table 3 leads to structures that correspond closely to the expected reactants and products (based on direct geometry optimizations), with energy differences that are less than 2 kcal/mol in each case. Therefore, it is likely that the transition structure for the C456:3H$_2$O + 4EFP that is described in Table 3 is a good approximation to the true TS.

The TDPBE0/DH(d,p) absorption, adiabatic, and fluorescence energies for the enol and keto tautomers of the molecular complexes are given in Tables 4 and 5, respectively. In C456, both absorption and fluorescence energies are higher in the enol tautomer than those for the corresponding keto tautomer by 1.26 and 1.31 eV, respectively, in the gas phase. In C456:3H$_2$O, both absorption and fluorescence energies are higher in the enol tautomer than those for the corresponding keto tautomer by 0.84 and 0.53 eV, respectively, in the gas phase. In general, the $\pi \rightarrow \pi^*$ vertical excitation, adiabatic, and vertical de-excitation energies of C456 with water molecules (C456:3H$_2$O and C456:3H$_2$O + 200EFP) are red-shifted in the enol tautomer and blue-shifted in the keto tautomer, relative to isolated C456. The global minimum structure of the excited-state enol tautomer of C456:3H$_2$O + 200EFP is given in Figure 6.
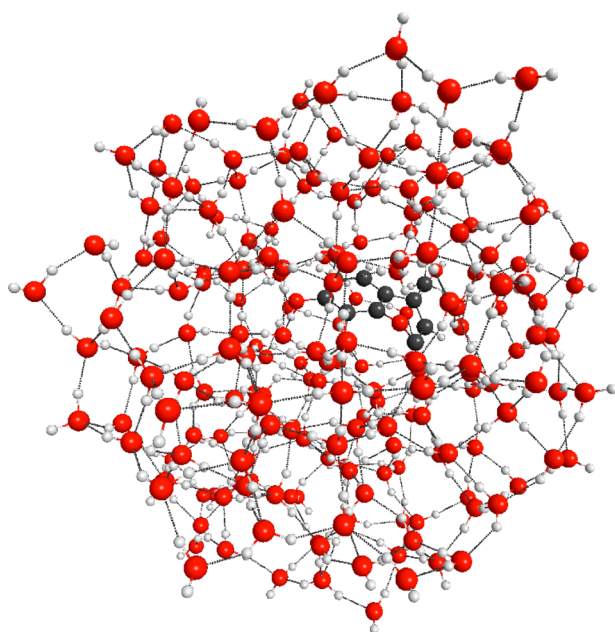
Figure 6. Global minima of the excited-state enol tautomer of C456:3H$_2$O in 200 EFP. The hydrogen, carbon, and oxygen atoms are colored white, black, and red, respectively.

4. CONCLUSIONS

The theoretical study of the ground-state and excited-state tautomerization reactions in C456 have been presented, using PBE0/DH(d,p) and TDPBE0/DH(d,p), respectively. The TSs of the HT reaction were found in C456:3H$_2$O and C456:3H$_2$O with PCM as well as in C456:3H$_2$O with small clusters of EFP waters. The optimized geometries of the corresponding tautomers are also presented. The TDPBE0/DH(d,p) ESP-derived charges along the excited-state IRC path predicts that the tautomerization reaction is a HT reaction, with hydrogen partial charges of ~0.55 e. The predicted activation energies are in excellent agreement with the experimental evidence. The

addition of water molecules to C456 assists the HT reaction by decreasing the activation energy in the excited state.

The results in the present work have also been compared with the previous theoretical data reported by Georgieva et al. on the C456:3H$_2$O system. They have considered the S$_1$ enol to keto tautomerization as a PT reaction; the barrier height was estimated to be 17−20 kcal/mol at the TDB3LYP/SVPD level of theory. In the present paper, the S$_1$ enol to keto tautomerization of C456:3H$_2$O was interpreted as a HT reaction (not a PT reaction), and the TDPBE0/DH(d,p) barrier height was calculated to be 10.15 kcal/mol (5.30 kcal/mol activation energy).

■ AUTHOR INFORMATION

Corresponding Author

*E-mail: mark@si.msg.chem.iastate.edu.

Notes

The authors declare no competing financial interest.

■ REFERENCES

(1) Douhal, A.; Kim, S. K.; Zewail, A. H. Femtosecond Molecular Dynamics of Tautomerization in Model Base Pairs. *Nature* **1995**, *378*, 260−263.

(2) Lu, D. S.; Voth, G. A. Proton Transfer in the Enzyme Carbonic Anhydrase: An Ab Initio Study. *J. Am. Chem. Soc.* **1998**, *120*, 4006−4014.

(3) Marx, D.; Tuckerman, M. E.; Hutter, J.; Parrinello, M. The Nature of the Hydrated Excess Proton in Water. *Nature* **1999**, *397*, 601−604.

(4) Agarwal, P. K.; Webb, S. P.; Hammes-Schiffer, S. Computational Studies of the Mechanism for Proton and Hydride Transfer in Liver Alcohol Dehydrogenase. *J. Am. Chem. Soc.* **2000**, *122*, 4803−4812.

(5) Geissler, P. L.; Dellago, C.; Chandler, D.; Hutter, J.; Parrinello, M. Autoionization in Liquid Water. *Science* **2001**, *291*, 2121−2124.

(6) Rini, M.; Magnes, B. Z.; Pines, E.; Nibbering, E. T. J. Real-Time Observation of Bimodal Proton Transfer in Acid−Base Pairs in Water. *Science* **2003**, *301*, 349−352.

(7) Zimmer, M. Green Fluorescent Protein (GFP): Applications, Structure, and Related Photophysical Behavior. *Chem. Rev.* **2002**, *102*, 759−781.

(8) Stoner-Ma, D.; Jaye, A. A.; Matousek, P.; Towrie, M.; Meech, S. R.; Tonge, P. J. Observation of Excited-State Proton Transfer in Green Fluorescent Protein Using Ultrafast Vibrational Spectroscopy. *J. Am. Chem. Soc.* **2005**, *127*, 2864−2865.

(9) Eikerling, M.; Kornyshev, A. A.; Kucernak, A. R. Water in Polymer Electrolyte Fuel Cells: Friend or Foe? *Phys. Today* **2006**, *59*, 38−44.

(10) Taylor, C. A.; El-bayoum, M. A.; Kasha, M. Excited-State 2-Proton Tautomerism in Hydrogen-Bonded N-Heterococlic Base Pairs. *Proc. Natl. Acad. Sci. U.S.A.* **1969**, *63*, 253−260.

(11) Manca, C.; Tanner, C.; Leutwyler, S. Excited State Hydrogen Atom Transfer in Ammonia−Wire and Water−Wire Clusters. *Int. Rev. Phys. Chem.* **2005**, *24*, 457−488.

(12) Kyrychenko, A.; Waluk, J. Excited-State Proton Transfer Through Water Bridges and Structure of Hydrogen-Bonded Complexes in 1*H*-Pyrrolo[3,2-*h*]quinoline: Adiabatic Time-Dependent Density Functional Theory Study. *J. Phys. Chem. A* **2006**, *110*, 11958−11967.

(13) Tanner, C.; Manca, C.; Leutwyler, S. Probing the Threshold to H Atom Transfer Along a Hydrogen-Bonded Ammonia Wire. *Science* **2003**, *302*, 1736−1739.

(14) Fernandez-Ramos, A.; Martinez-Nunez, E.; Vazquez, S. A.; Rios, M. A.; Estevez, C. M.; Merchan, M.; Serrano-Andres, L. Hydrogen

Transfer vs Proton Transfer in 7-Hydroxy-Quinoline (NH₃)₃: A CASSCF/CASPT2 Study. *J. Phys. Chem. A* **2007**, *111*, 5907−5912.

(15) Gordon, M. S. Hydrogen Transfer in 7-Azaindole. *J. Phys. Chem.* **1996**, *100*, 3974−3979.

(16) Chaban, G. M.; Gordon, M. S. The Ground and Excited State Hydrogen Transfer Potential Energy Surface in 7-Azaindole. *J. Phys. Chem. A* **1998**, *103*, 185−189.

(17) Atkins, R. L.; Bliss, D. E. Substituted Coumarins and Azacoumarins — Synthesis and Fluorescent Properties. *J. Org. Chem.* **1978**, *43*, 1975−1980.

(18) Schimitschek, E. J.; Trias, J. A.; Hammond, P. R.; Henry, R. A.; Atkins, R. L. New Laser Dyes with Blue−Green Emission. *Opt. Commun.* **1976**, *16*, 313−316.

(19) Reynolds, G. A.; Drexhage, K. H. New Coumarin Dyes with Rigidized Structure for Flashlamp-Pumped Dye Lasers. *Opt. Commun.* **1975**, *13*, 222−225.

(20) Rechthaler, K.; Kohler, G. Excited-State Properties and Deactivation Pathways of 7-Aminocoumarins. *Chem. Phys.* **1994**, *189*, 99−116.

(21) Jones, G.; Jackson, W. R.; Choi, C.; Bergmark, W. R. Solvent Effects on Emission Yield and Lifetime for Coumarin Laser Dyes — Requirements for a Rotatory Decay Mechanism. *J. Phys. Chem.* **1985**, *89*, 294−300.

(22) Jones, G.; Jackson, W. R.; Kanoktanaporn, S.; Halpern, A. M. Solvent Effects on Photophysical Parameters for Coumarin Laser Dyes. *Opt. Commun.* **1980**, *33*, 315−320.

(23) Drexhage, K. H. *Dye-Lasers*; Springer-Verlag: New York, 1990.

(24) McCarthy, P. K.; Blanchard, G. J. AM1 Study of the Electronic Structure of Coumarins. *J. Phys. Chem.* **1993**, *97*, 12205−12209.

(25) Jones, G.; Jimenez, J. A. C. Azole-Linked Coumarin Dyes as Fluorescence Probes of Domain-Forming Polymers. *J. Photochem. Photobiol., B* **2001**, *65*, 5−12.

(26) Moriya, T. Excited-State Reactions of Coumarins in Aqueous Solutions. III. The Fluorescence Quenching of 7-Ethoxycoumarins by the Chloride Ion in Acidic Solutions. *Bull. Chem. Soc. Jpn.* **1986**, *59*, 961−968.

(27) Kaholek, M.; Hrdlovič, P. Spectral Properties of Coumarin Derivatives Substituted at Position 3. Effect of Polymer Matrix. *J. Photochem. Photobiol., A* **1997**, *108*, 283−288.

(28) Raju, B. B.; Costa, S. M. B. Excited-State Behavior of 7-Diethylaminocoumarin Dyes in AOT Reversed Micelles: Size Effects. *J. Phys. Chem. B* **1999**, *103*, 4309−4317.

(29) Moylan, C. R. Molecular Hyperpolarizabilities of Coumarin Dyes. *J. Phys. Chem.* **1994**, *98*, 13513−13516.

(30) Fink, D. W.; Koehler, W. R. pH Effects on Fluorescence of Umbelliferone. *Anal. Chem.* **1970**, *42*, 990−993.

(31) Shank, C. V.; Dienes, A.; Trozzolo, A. M.; Myer, J. A. Near UV to Yellow Tunable Laser Emission from an Organic Dye. *Appl. Phys. Lett.* **1970**, *16*, 405−407.

(32) Dienes, A.; Shank, C. V.; Trozzolo, A. M. Evidence for Exciplex Laser Action in Coumarin Dyes by Measurements of Stimulated Fluorescence. *Appl. Phys. Lett.* **1970**, *17*, 189−191.

(33) Schulman, S. G.; Rosenberg, L. S. Tautomerization Kinetics of 7-Hydroxy-4-methylcoumarin in the Lowest Excited Singlet State. *J. Phys. Chem.* **1979**, *83*, 447−451.

(34) Trozzolo, A. M.; Dienes, A.; Shank, C. V. Excited-State Reactions of a Laser Dye. Evidence for a Two-Step Phototautomerism in 7-Hydroxy-4-methylcoumarin. *J. Am. Chem. Soc.* **1974**, *96*, 4699−4700.

(35) Seixas de Melo, J. S.; Becker, R. S.; Macanita, A. L. Photophysical Behavior of Coumarins as a Function of Substitution and Solvent: Experimental Evidence for the Existence of a Lowest Lying ¹(n,π*) State. *J. Phys. Chem.* **1994**, *98*, 6054−6058.

(36) Moriya, T. Excited-State Reactions of Coumarins. VII. The Solvent-Dependent Fluorescence of 7-Hydroxycoumarins. *Bull. Chem. Soc. Jpn.* **1988**, *61*, 1873−1886.

(37) Moriya, T. Excited-State Reactions of Coumarins in Aqueous-Solutions. I. The Phototautomerization of 7-Hydroxycoumarin and Its Derivative. *Bull. Chem. Soc. Jpn.* **1983**, *56*, 6−14.

(38) Kobayashi, T. Picosecond Kinetics of 4-Methylumbelliferone Fluorescence Observed with Mode-Locked Laser and Streak Camera. *J. Phys. Chem.* **1978**, *82*, 2277−2281.

(39) Bardez, E.; Boutin, P.; Valeur, B. Photoinduced Biprotonic Transfer in 4-Methylumbelliferone. *Chem. Phys. Lett.* **1992**, *191*, 142−148.

(40) Georgieva, I.; Trendafilova, N.; Aquino, A. J. A.; Lischka, H. Excited State Properties of 7-Hydroxy-4-methylcoumarin in the Gas Phase and in Solution. A Theoretical Study. *J. Phys. Chem. A* **2005**, *109*, 11860−11869.

(41) Miertus, S.; Scrocco, E.; Tomasi, J. Electrostatic Interaction of a Solute with a Continuum — A Direct Utilization of Abinitio Molecular Potentials for the Prevision of Solvent Effects. *Chem. Phys.* **1981**, *55*, 117−129.

(42) Tomasi, J.; Persico, M. Molecular Interactions in Solution: An Overview of Methods Based on Continuous Distributions of the Solvent. *Chem. Rev.* **1994**, *94*, 2027−2094.

(43) Georgieva, I.; Trendafilova, N.; Aquino, A. J. A.; Lischka, H. Excited-State Proton Transfer in 7-Hydroxy-4-methylcoumarin Along a Hydrogen-Bonded Water Wire. *J. Phys. Chem. A* **2007**, *111*, 127−135.

(44) Day, P. N.; Jensen, J. H.; Gordon, M. S.; Webb, S. P.; Stevens, W. J.; Krauss, M.; Garmer, D.; Basch, H.; Cohen, D. An Effective Fragment Method for Modeling Solvent Effects in Quantum Mechanical Calculations. *J. Chem. Phys.* **1996**, *105*, 1968−1986.

(45) Gordon, M. S.; Freitag, A. M.; Bandyopadhyay, P.; Jensen, J. H.; Kairys, V.; Stevens, W. J. The Effective Fragment Potential Method: A QM-Based MM Approach to Modeling Environmental Effects in Chemistry. *J. Phys. Chem. A* **2001**, *105*, 293−307.

(46) Adamovic, I.; Freitag, M. A.; Gordon, M. S. Density Functional Theory Based Effective Fragment Potential Method. *J. Chem. Phys.* **2003**, *118*, 6725−6732.

(47) Perdew, J. P.; Burke, K.; Ernzerhof, M. Generalized Gradient Approximation Made Simple. *Phys. Rev. Lett.* **1996**, *77*, 3865−3868.

(48) Perdew, J. P.; Burke, K.; Ernzerhof, M. Generalized Gradient Approximation Made Simple. *Phys. Rev. Lett.* **1997**, *78*, 1396−1396.

(49) Adamo, C.; Barone, V. Toward Reliable Density Functional Methods without Adjustable Parameters: The PBE0 Model. *J. Chem. Phys.* **1999**, *110*, 6158−6170.

(50) Ishida, K.; Morokuma, K.; Komornicki, A. The Intrinsic Reaction Coordinate. An Ab Initio Calculation for HNC → HCN and H⁻ + CH₄ → CH₄ + H⁻. *J. Chem. Phys.* **1977**, *66*, 2153−2156.

(51) Muller, K. Reaction Paths on Multidimensional Energy Hypersurfaces. *Angew. Chem., Int. Ed. Engl.* **1980**, *19*, 1−13.

(52) Schmidt, M. W.; Gordon, M. S.; Dupuis, M. The Intrinsic Reaction Coordinate and the Rotational Barrier in Silaethylene. *J. Am. Chem. Soc.* **1985**, *107*, 2585−2589.

(53) Garrett, B. C.; Redmon, M. J.; Steckler, R.; Truhlar, D. G.; Baldridge, K. K.; Bartol, D.; Schmidt, M. W.; Gordon, M. S. Algorithms and Accuracy Requirements for Computing Reaction Paths by the Method of Steepest Descent. *J. Phys. Chem.* **1988**, *92*, 1476−1488.

(54) Baldridge, K. K.; Gordon, M. S.; Steckler, R.; Truhlar, D. G. Ab Initio Reaction Paths and Direct Dynamics Calculations. *J. Phys. Chem.* **1989**, *93*, 5107−5119.

(55) Gonzales, C.; Schlegel, H. B. An Improved Algorithm for Reaction Path Following. *J. Chem. Phys.* **1989**, *90*, 2154−2161.

(56) Singh, U. C.; Kollman, P. A. An Approach to Computing Electrostatic Charges for Molecules. *J. Comput. Chem.* **1984**, *5*, 129−145.

(57) Bayly, C. I.; Cieplak, P.; Cornell, W. D.; Kollman, P. A. A Well-Behaved Electrostatic Potential Based Method Using Charge Restraints for Deriving Atomic Charges: The RESP Model. *J. Phys. Chem.* **1993**, *97*, 10269−10280.

(58) Day, P. N.; Pachter, R.; Gordon, M. S.; Merrill, G. N. A Study of Water Clusters Using the Effective Fragment Potential and Monte Carlo Simulated Annealing. *J. Chem. Phys.* **2000**, *112*, 2063−2073.

H

dx.doi.org/10.1021/jp404686c | *J. Phys. Chem. B* XXXX, XXX, XXX−XXX

(59) Metropolis, N.; Rosenbluth, A. W.; Rosenbluth, M. N.; Teller, A. H.; Teller, E. Equation of State Calculations by Fast Computing Machines. *J. Chem. Phys.* **1953**, *21*, 1087−1092.

(60) Kirkpatrick, S.; Gelatt, C. D.; Vecchi, M. P. Optimization by Simulated Annealing. *Science* **1983**, *220*, 671−680.

(61) Schmidt, M. W.; Baldridge, K. K.; Boatz, J. A.; Elbert, S. T.; Gordon, M. S.; Jensen, J. H.; Koseki, S.; Matsunaga, N.; Nguyen, K. A.; Su, S.; et al. General Atomic and Molecular Electronic Structure System. *J. Comput. Chem.* **1993**, *14*, 1347−1363.

(62) Gordon, M. S.; Schmidt, M. W. *Advances in Electronic Structure Theory: GAMESS a Decade Later*. Elsevier: Amsterdam, The Netherlands, 2005.

(63) Bode, B. M.; Gordon, M. S. MacMolPlt: A Graphical User Interface for GAMESS. *J. Mol. Graphics Modell.* **1998**, *16*, 133−138.

(64) Tanner, C.; Manca, C.; Leutwyler, S. Exploring Excited-State Hydrogen Atom Transfer Along an Ammonia Wire Cluster: Competitive Reaction Paths and Vibrational Mode Selectivity. *J. Chem. Phys.* **2005**, *122*, 204326−204336.